Supplementary Information for

Extremely Poleward Shift of Antarctic Circumpolar Current by Eccentricity during the Last Interglacial

Lijuan Lu, Xufeng Zheng*, Michael E. Weber, Victoria Peck, Brendan T. Reilly, Zhong Chen, Wen Yan, Tianyu Chen, Hong Yan, Xun Gong, Shuzhuang Wu, Liwei Zheng, Shiming Wan, Yan Du, Lisa Tauxe, Qinghua Yang, Stefanie Brachfeld, Trevor Williams, Yasmina M. Martos, Zhiheng Du, Marga Garcia, Lara F. Pérez, Hu Yang, Bingyue Huang, Jonathan Warnock, and Shuh-Ji Kao*

* Correspondence to: X. Z. and S. K. (xufengzheng@hainanu.edu.cn; sjkao@ hainanu.edu.cn).

This file includes:

- Supplementary Figs. 1-19;
- Supplementary Tables 1-2;
- References.

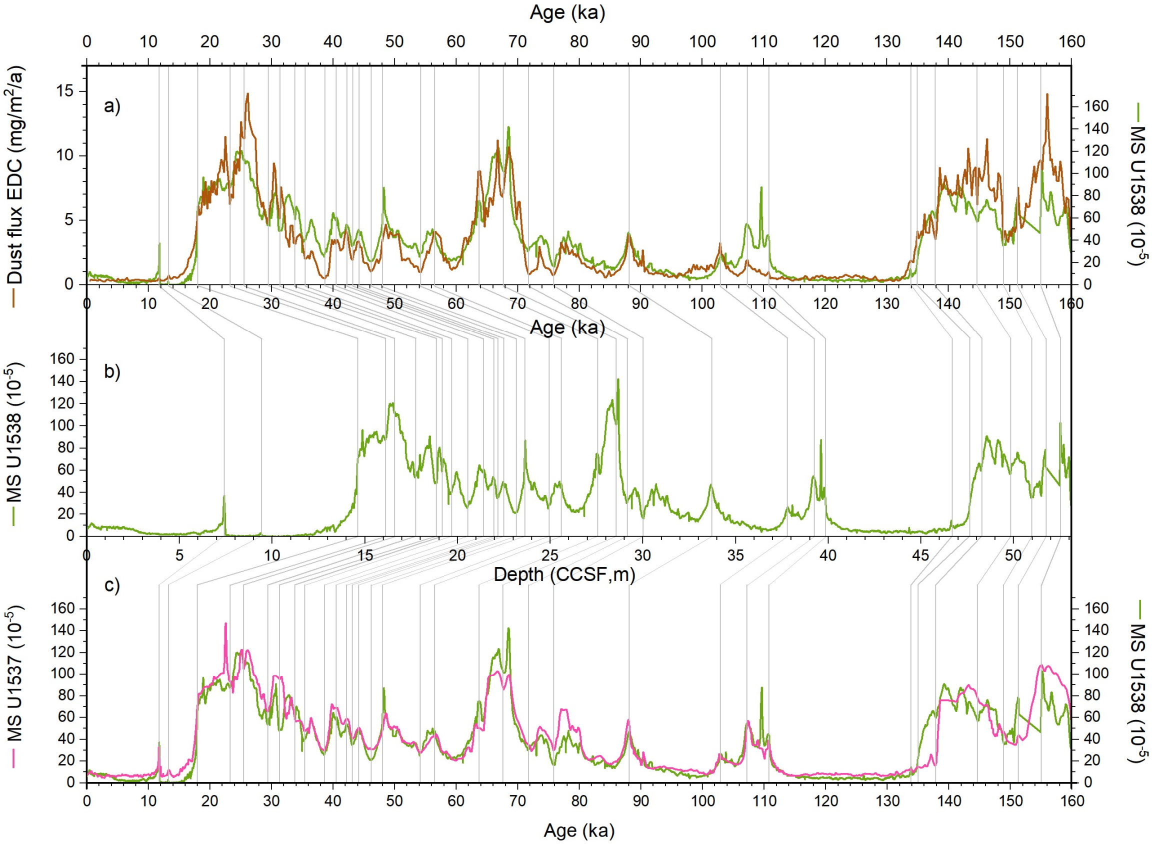

Supplementary Fig. 1 | Age model of Site U1538. a) Correlation of U1538 magnetic susceptibility (MS) to EPICA Dome C (EDC) dust flux[1,2]. **b)** U1538 MS[1]. **c)** Correlation of U1538 MS to U1537 MS on the AICC 2012 age scale[1,2,3].

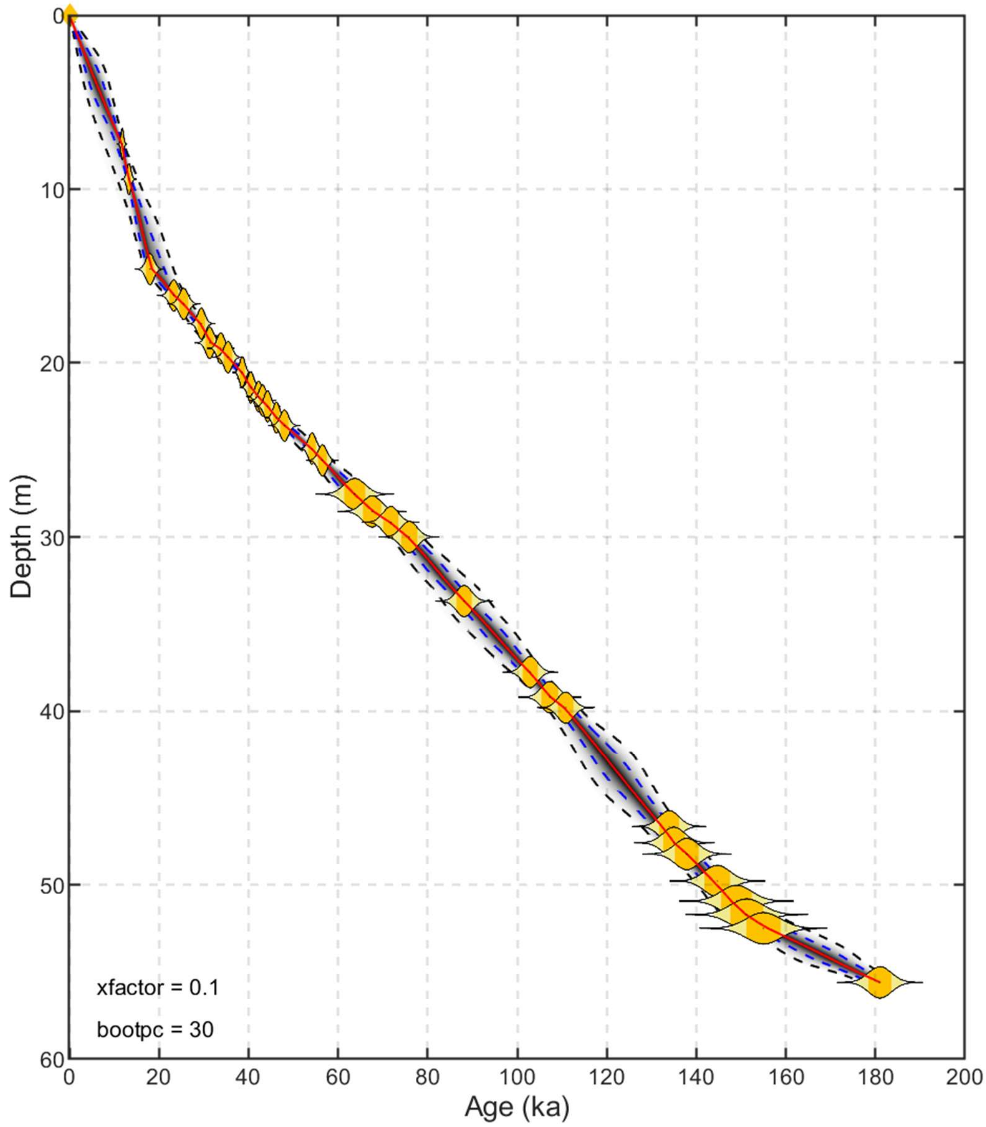

Supplementary Fig. 2 | Age model of Site U1538 conducted by the Undatable MATLAB tool[4].

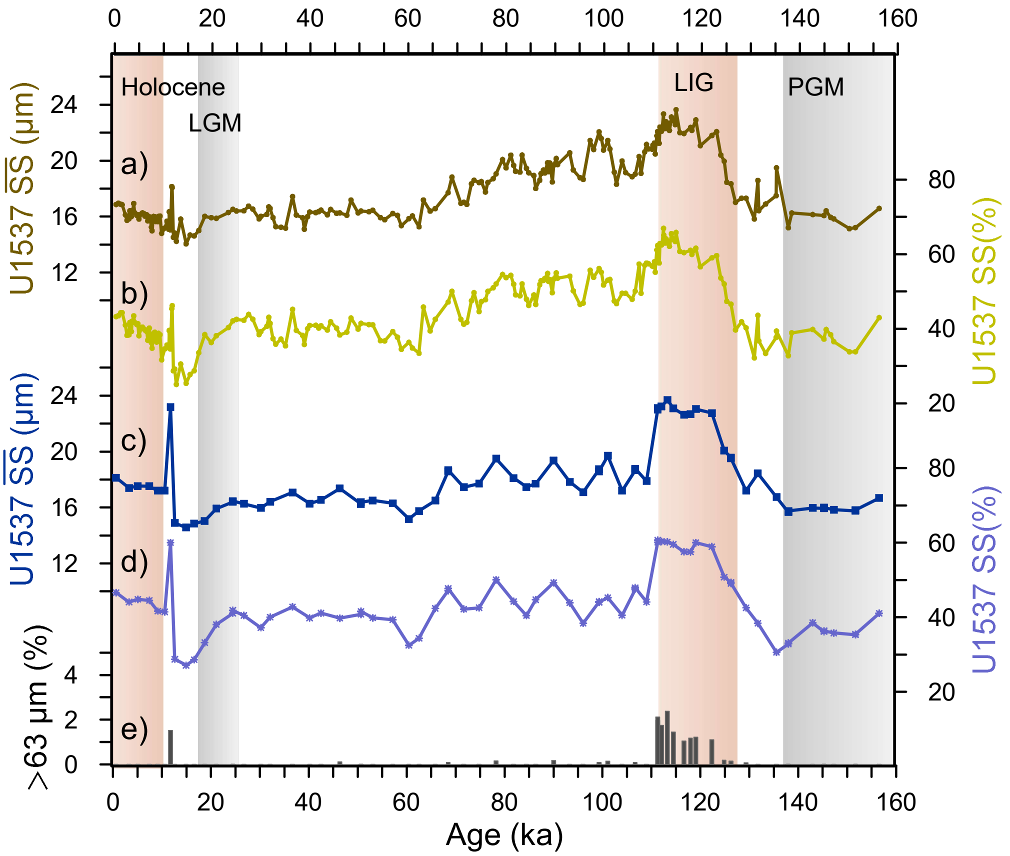

Supplementary Fig. 3 | Results of grain-size measurements at Site U1537. a) and **b)** are $\overline{SS}$ and SS% in Group One of U1537, respectively. **c)** and **d)** are $\overline{SS}$ and SS% in Group Two of U1537, respectively. **e**) The percentage of grain size larger than 63 μm in Group Two of U1537; LGM = Last Glacial Maximum; PGM = Penultimate Glacial Maximum.

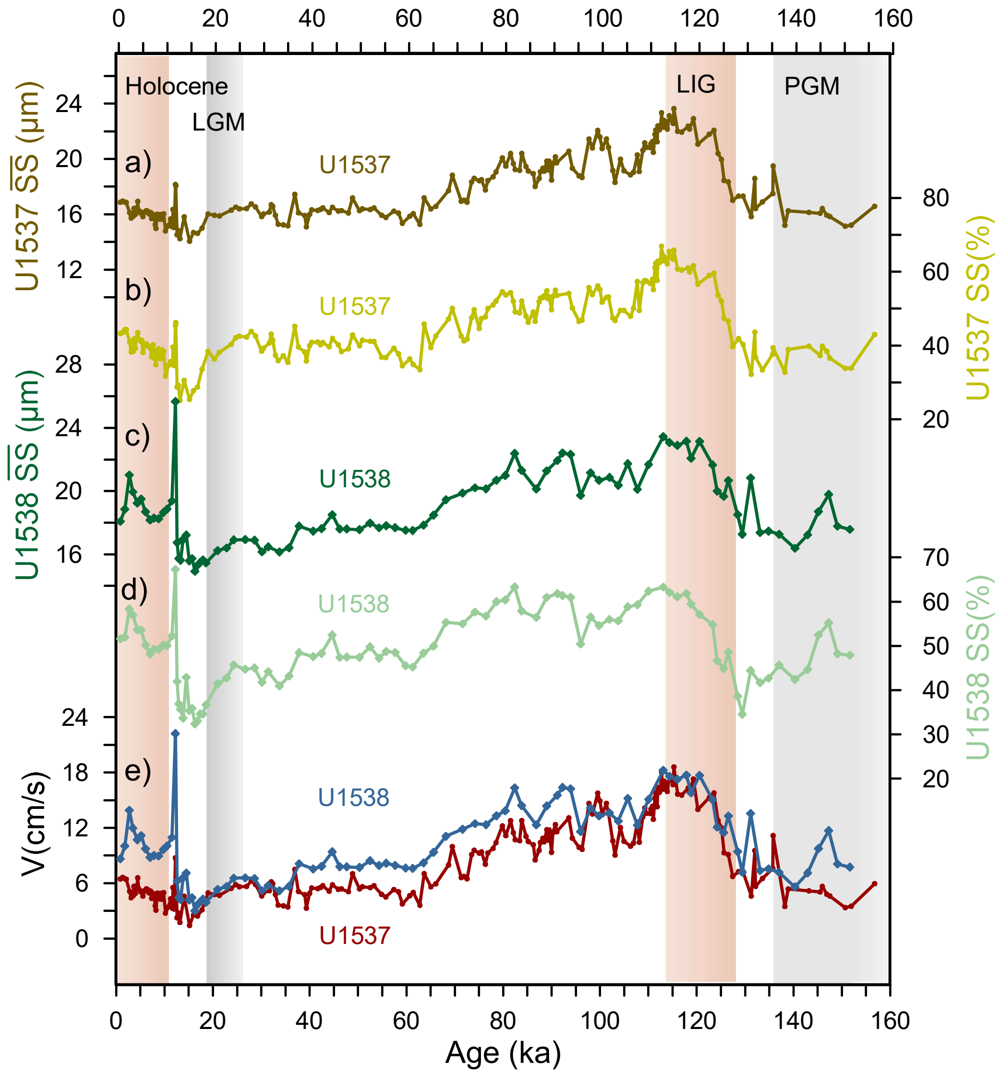

Supplementary Fig. 4 | Results of grain-size measurements at Sites U1537 and U1538. a) and **b)** are $\overline{SS}$ and SS% in Group One of Site U1537, respectively. **c)** and **d)** are $\overline{SS}$ and SS% at Site U1538, respectively. **e)** U1537 and U1538 bottom flow speeds estimated by the relationship between $\overline{SS}$ and bottom current speed in the Scotia-Weddell Sea region[5,6], respectively.

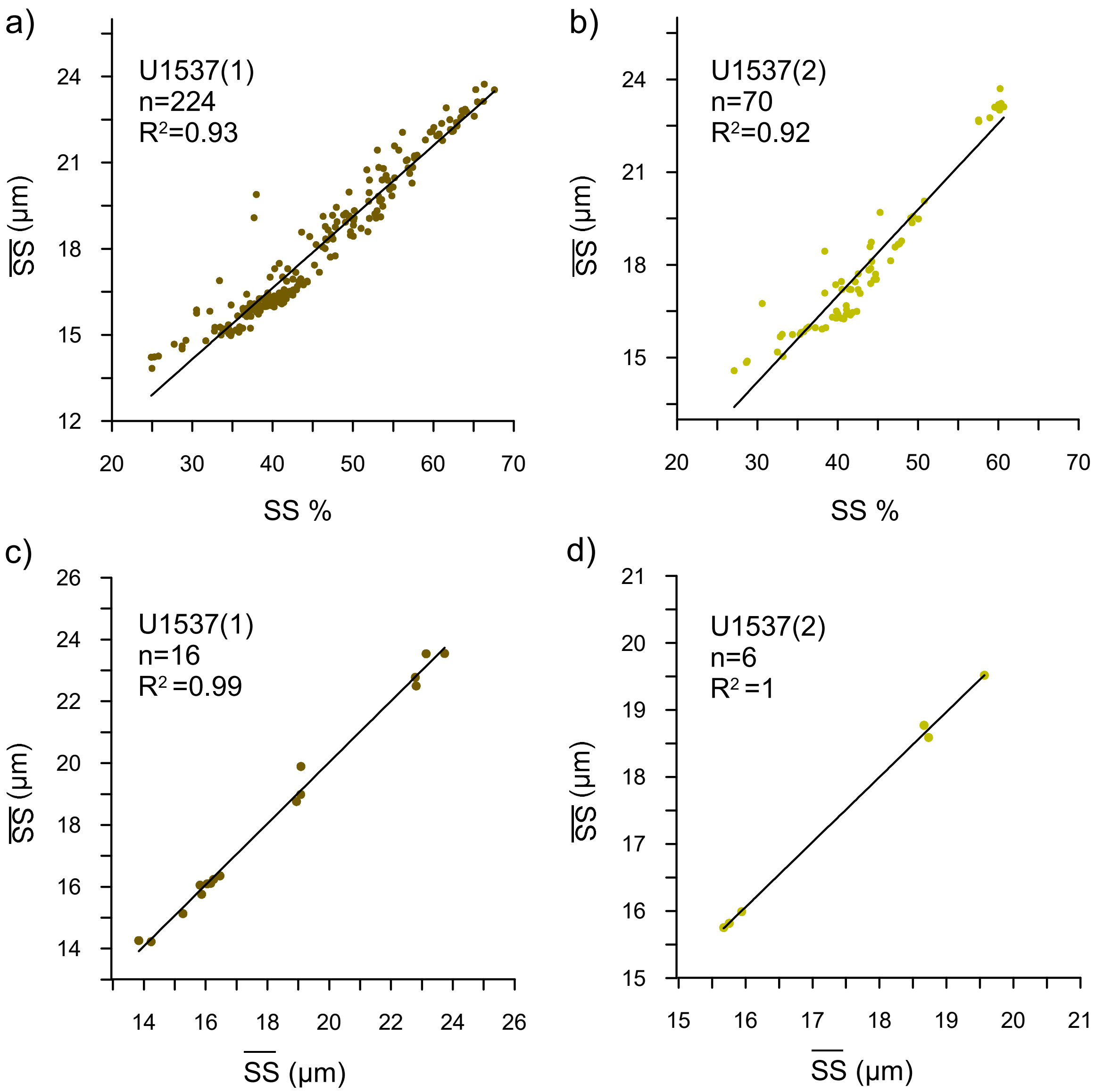

Supplementary Fig. 5 | Results of $\overline{SS}$ at Site U1537. a) and **b)** are the correlation between $\overline{SS}$ and SS% in Group One and Group Two of U1537, respectively. **c)** and **d)** are the repeated results of $\overline{SS}$ in Group One and Group Two of Site U1537, respectively.

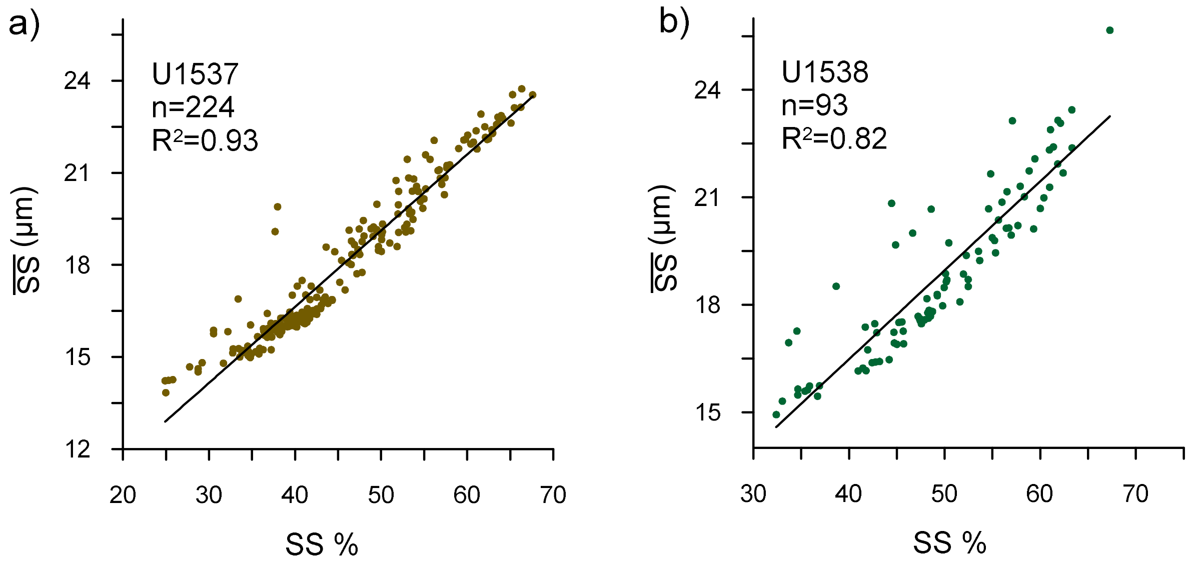

Supplementary Fig. 6 | Correlation between $\overline{SS}$ and SS% at Site U1537 (a) and Site U1538 (b), respectively.

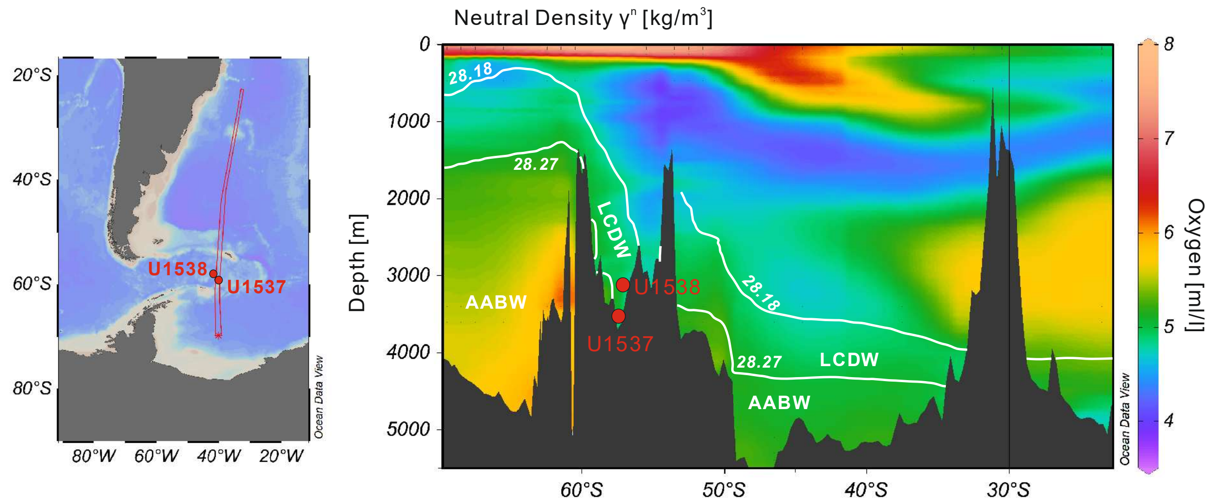

Supplementary Fig. 7 | Color-mapped oxygen concentrations, with neutral density contours (γ^n) overlain, from the 2013 Annual World Ocean Atlas by Ocean Data Views[7,8,9]. The left figure defines the section crossing Sites U1537 and U1538. The isopycnal with a neutral density of 28.27 kg m^{-3} separates the water mass of AABW from the overlying Lower Circumpolar Deep Water (LCDW)[10]. The isopycnal with a neutral density of 28.18 kg m^{-3} marks the top of the Antarctic Circumpolar Current bottom water[11].

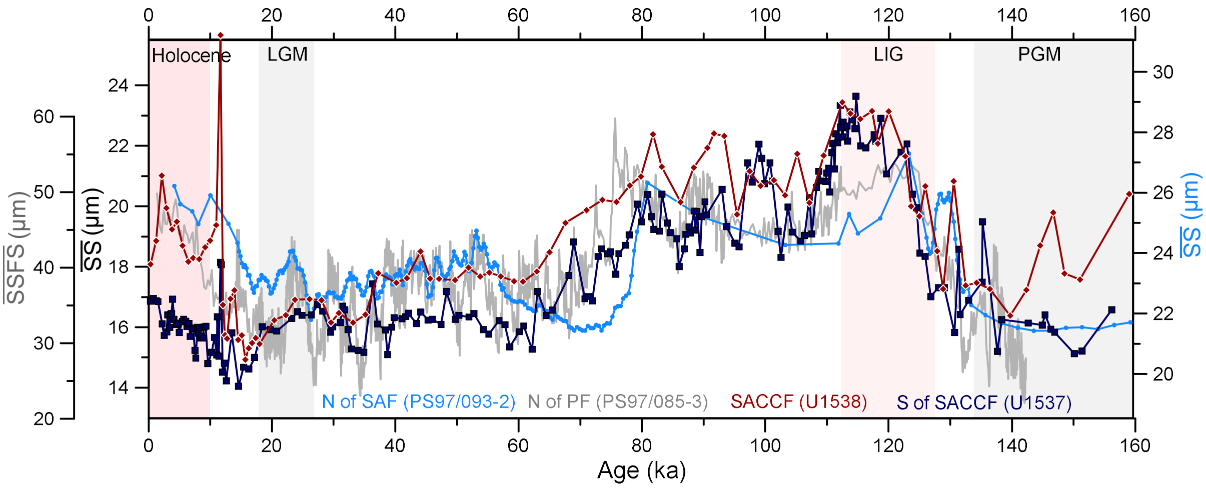

Supplementary Fig. 8 | Comparisons of ACC records within the Scotia Sea and the Drake Passage. $\overline{SSFS}$ at Site PS97/085-3[12] (gray), $\overline{SS}$ at Site PS97/093-2[13] (light blue), $\overline{SS}$ at Sites U1538 (red) and U1537 (dark blue).

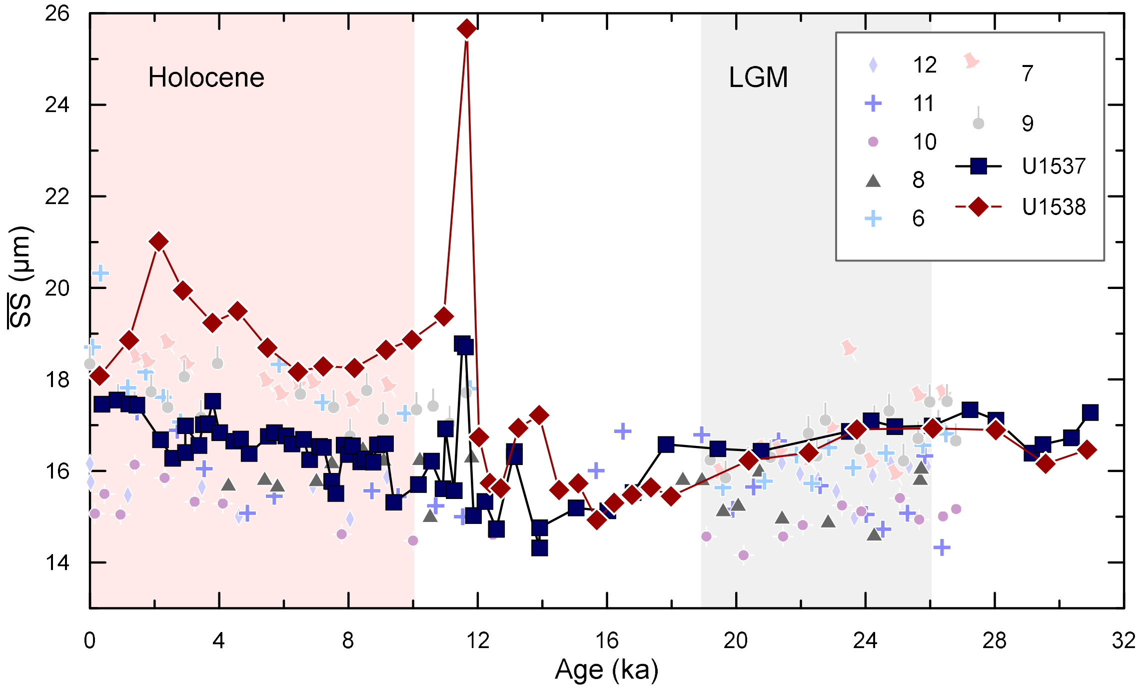

Supplementary Fig. 9 | Comparisons of $\overline{SS}$ in the Scotia Sea over the past 32 ka. For details on the cores (6-12), please refer to Fig. 1 or McCave et al. (2014)[14].

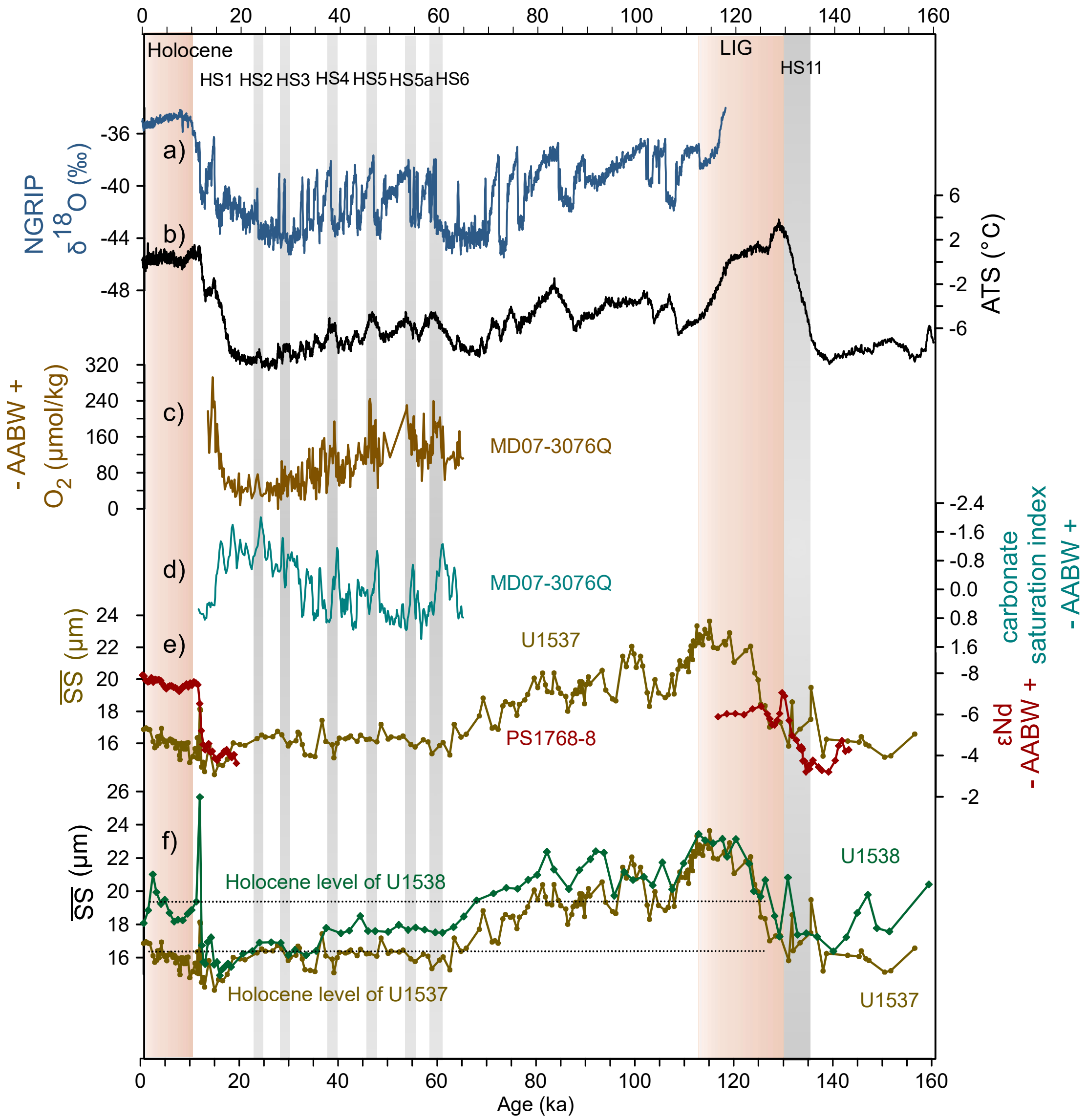

Supplementary Fig. 10 | Comparisons of $\overline{SS}$ with the associated AABW records over the past 160 ka. a) Oxygen isotope record of the North Greenland Ice Core Project (NGRIP) ice core[15,16]. **b)** ATS[17]. **c)** Bottom water $[O_2]$ at Site MD07-3076Q[18]. **d)** Carbonate saturation index at Site MD07-3076Q[19]. **e)** $\overline{SS}$ at Site U1537 (this study) and Nd isotope records at Site PS1768-8[20]. **f)** $\overline{SS}$ at Sites U1537 and U1538 (this study). HS=Heinrich Stadials.

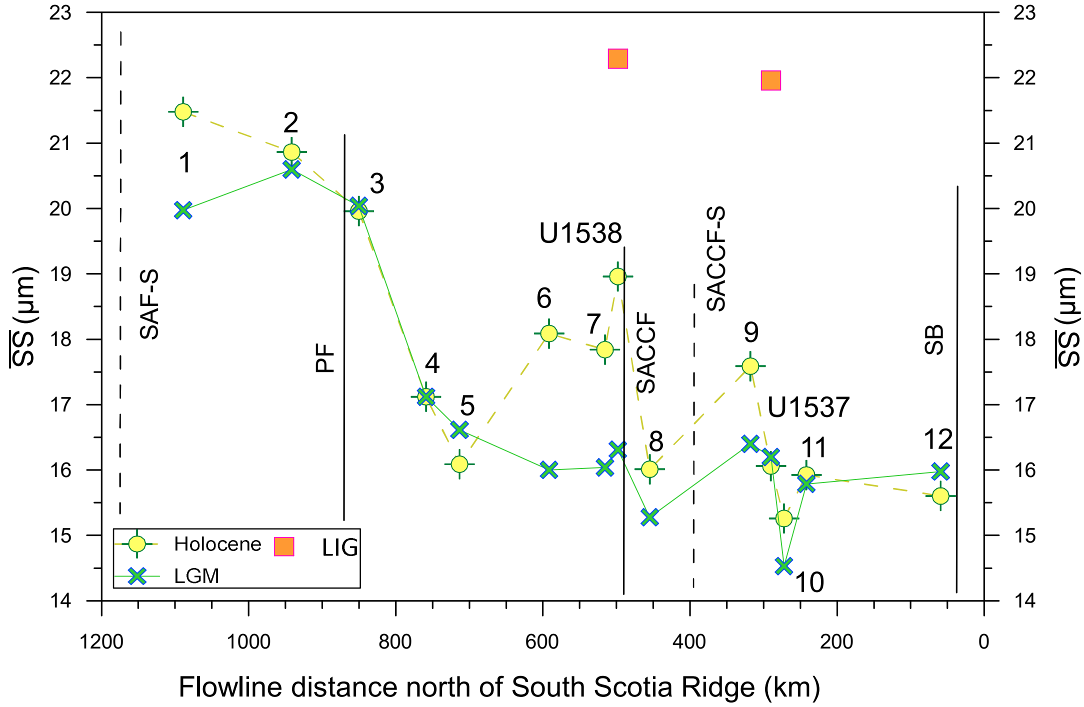

Supplementary Fig. 11 | Comparisons of $\overline{SS}$ in the Scotia Sea during the Holocene, LGM, and LIG. For details of the cores (1-12), refer to Fig. 1 or McCave et al. (2014)[14].

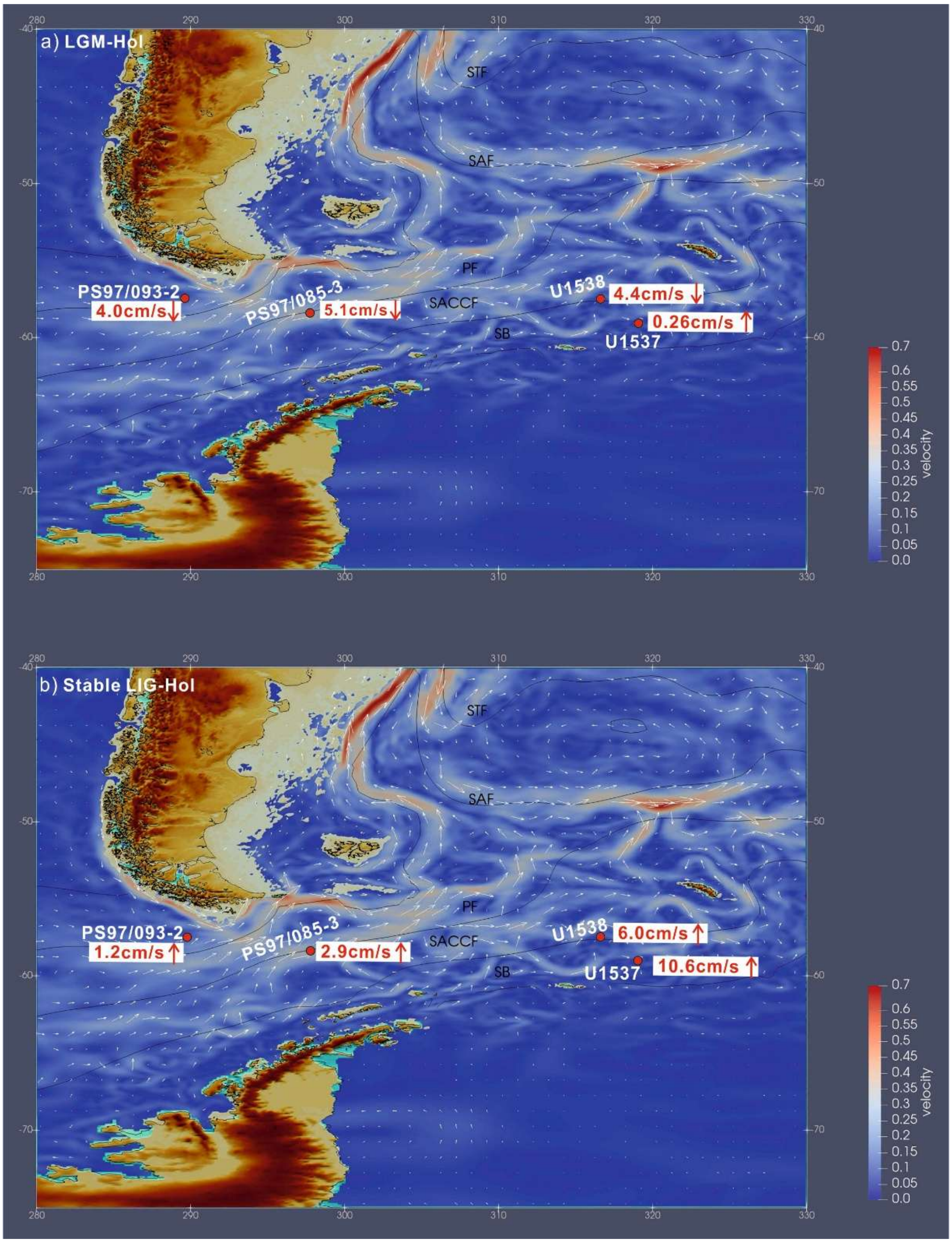

Supplementary Fig. 12 | Comparisons of ACC speeds in the Scotia Sea and Drake Passage[12,13] between the Last Glacial Maximum (LGM) and Holocene (Hol) (a), and between the LIG and Hol (b). Base map using the MDT_CNES_CLS18_global data set[21] shows the global ocean surface current, with warmer red colors representing higher current speeds.

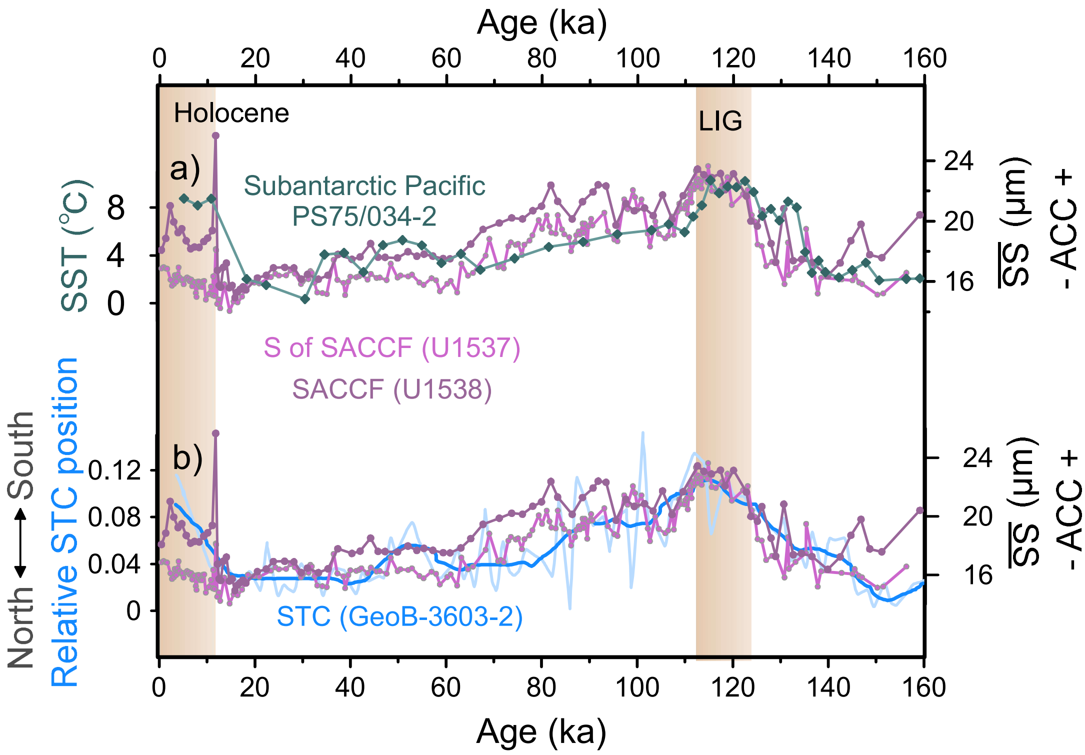

Supplementary Fig. 13 | The comparisons of $\overline{SS}$ at Sites U1537 and U1538 with Sea Surface Temperature (SST) record at subantarctic Pacific (PS75/034-2)[22] and relative STC position, derived from the ratio of G. truncatulinoides / (N. pachyderma (dex.) + G. inflata + G. truncatulinoides) in the southern Cape Basin (GeoB-3603-2)[23]

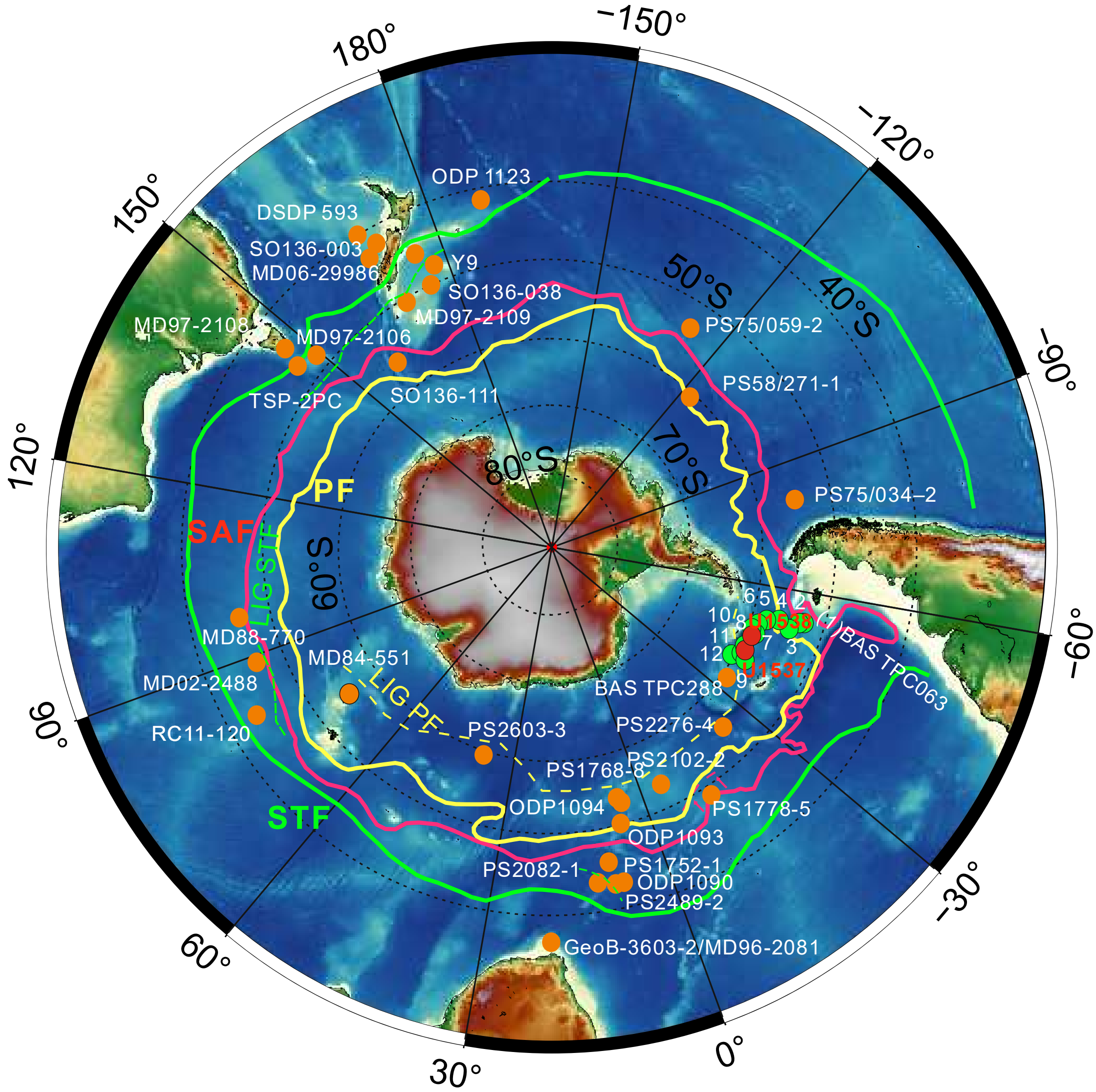

Supplementary Fig. 14 | Shift of ACC fronts during Last Interglacial. The solid green, red, and light yellow lines indicate the STF, SAF, and PF, respectively[11]. The dashed green and light yellow lines reflect the STF and SAF during the LIG, respectively.

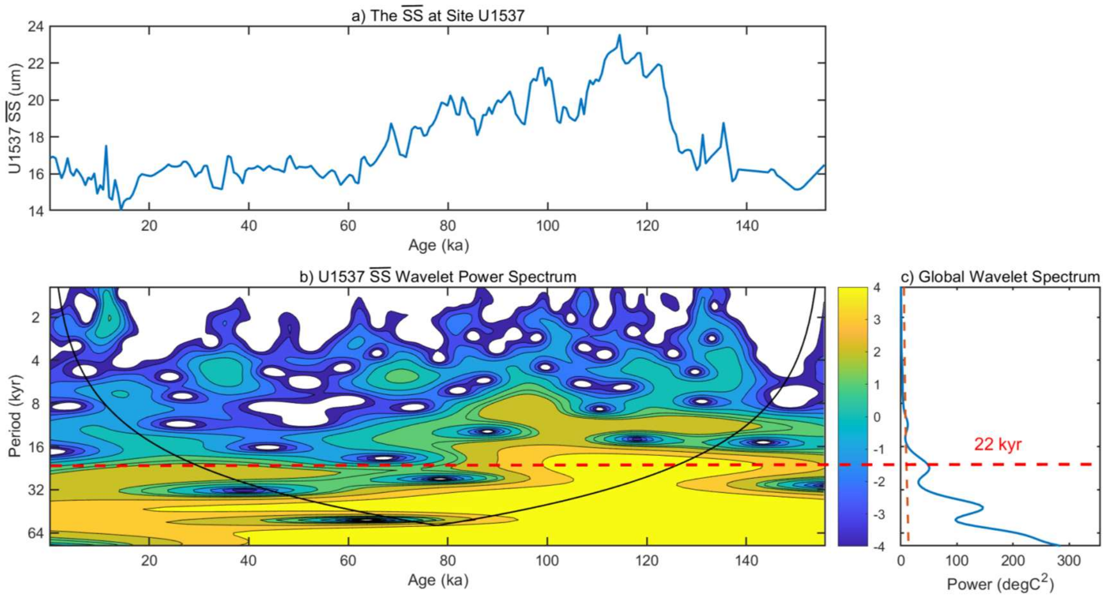

Supplementary Fig. 15 | Wavelet analysis for standardized $\overline{SS}$ based on Torrence and Compo (1998)[24]. a) U1537 $\overline{SS}$ interpolated in the sample rate of 0.5962 kyr. **b)** Wavelet spectrum for 1537 $\overline{SS}$ using the Morlet wavelet. **c)** Global wavelet spectrum. The black thick contour in **b)** and dashed thin red line in **c)** are the 95% confidence level against red noise.

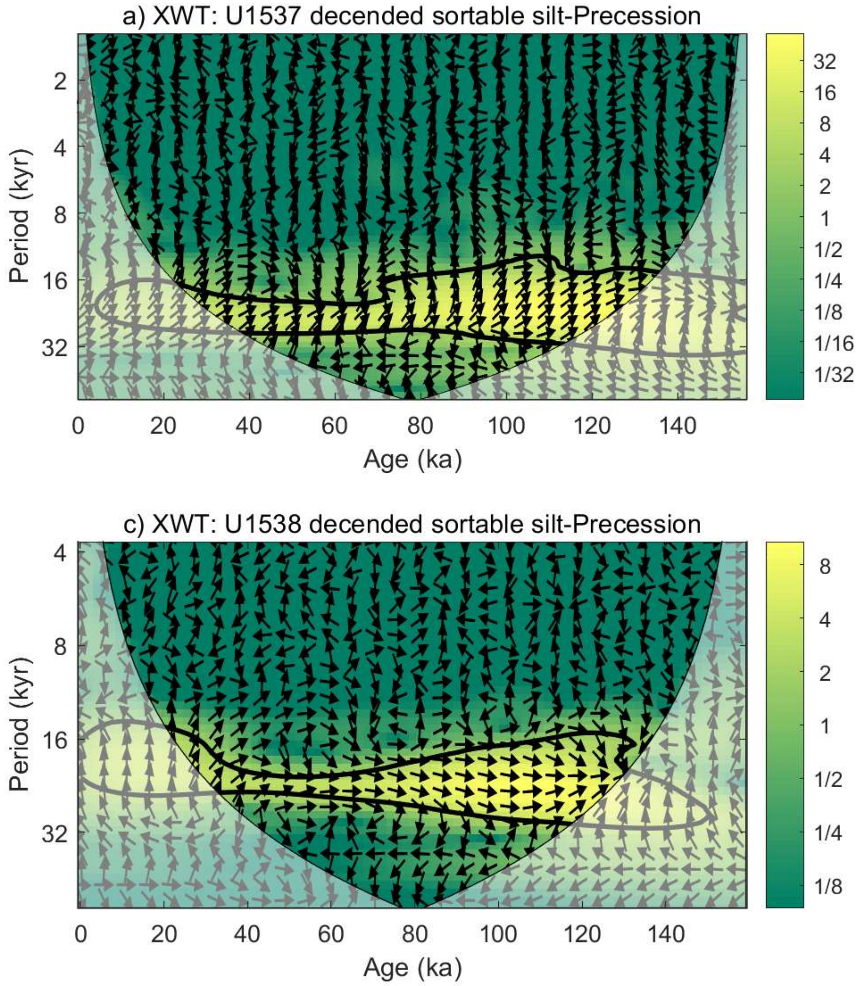

Supplementary Fig. 16 | Cross-wavelet transform (XWT) spectrum of detrended $\overline{SS}$ and precession index[25]. The black thick line of statistical significance designates the 95% confidence level against red noise. The right color bar indicates the power. The phase relationship is indicated by the arrows, with right arrows indicating "in-phase" and left arrows indicating "anti-phase" relationships.

101

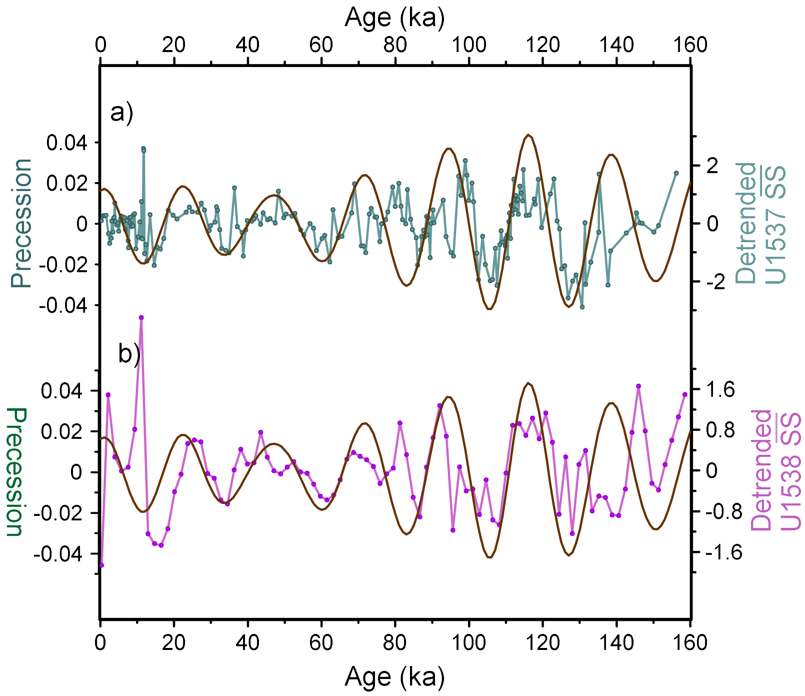

102 **Supplementary Fig. 17 | Comparison of detrended $\overline{SS}$ at Site U1537 and U1538**

103 **with precession index**[25].

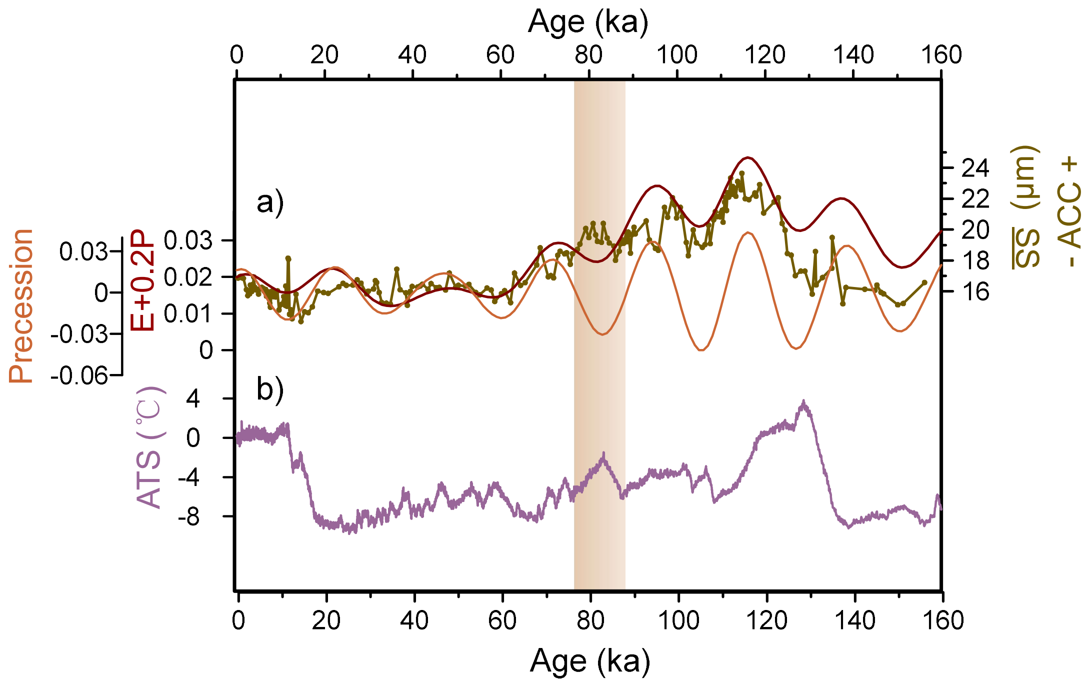

Supplementary Fig. 18 | Comparision of grain size at Site U1537 with orbital parameters and Antarctic Temperature. a) Eccentricity (E)+0.2 precession (P) [25], precession[25] and $\overline{SS}$ at Site U1537; b) Antarcitc temperature stack[17].

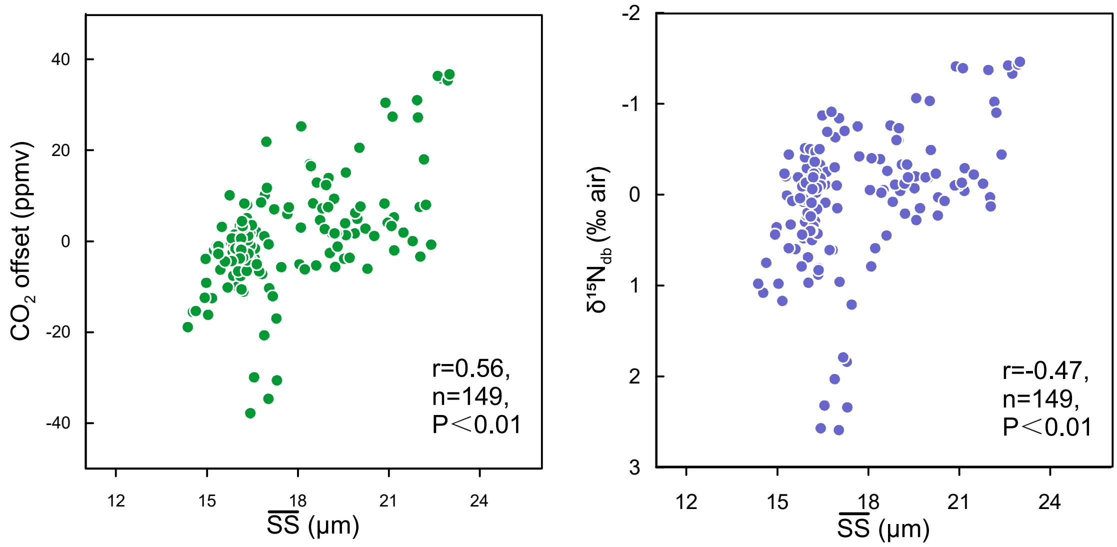

Supplementary Fig. 19 | Correlation of U1537 $\overline{SS}$ record, the CO_2[26] and $\delta^{15}N_{db}$ offset records[27]. Pearson correlation coefficients are *r* = 0.56 and *r* = –0.47, respectively.

Supplementary Table 1. Age control points for the construction of the age model for U1538

U1538 Depth CCSF (m)	U1538 Age (ka BP)	Age uncertainty (ka BP)	Dating method
0	0	0	1538 MS-EDC dust
7.414	11.78965	0.29254	1538 MS-EDC dust
9.427	13.26745	0.45259	1538 MS-EDC dust
14.603	17.96229	0.89579	1538 MS-EDC dust
16.114	23.29670	0.98313	1538 MS-EDC dust
16.6	25.5	0.99795	1538 MS-EDC dust
17.735	29.44417	0.81335	1538 MS-EDC dust
18.841	31.31958	0.89983	1538 MS-EDC dust
19.154	33.78699	0.81633	1538 MS-EDC dust
19.661	35.41029	0.91173	1538 MS-EDC dust
20.542	38.59196	0.60146	1538 MS-EDC dust
21.4	40.5	0.67896	1538 MS-EDC dust
21.932	42.20861	0.73499	1538 MS-EDC dust
22.155	43.13720	0.79250	1538 MS-EDC dust
22.488	44.23214	0.74947	1538 MS-EDC dust
23.142	46.18901	0.70392	1538 MS-EDC dust
23.6	48	0.93114	1538 MS-EDC dust
24.916	54.17565	0.81024	1538 MS-EDC dust
25.6	56.5	0.97243	1538 MS-EDC dust
27.536	63.72066	2.35817	1538 MS-EDC dust
28.533	67.59178	2.04820	1538 MS-EDC dust
29.151	71.75788	1.70166	1538 MS-EDC dust
30.002	75.86295	1.80209	1538 MS-EDC dust
33.694	88.13510	1.71239	1538 MS-EDC dust
37.771	102.91387	1.68251	1538 MS-EDC dust
39.214	107.26295	1.89157	1538 MS-EDC dust
39.817	110.81620	1.73168	1538 MS-EDC dust
46.656	133.91951	2.20442	1538 MS-EDC dust
47.6	135	2.42034	1538 MS-EDC dust
48.240	137.87303	2.64080	1538 MS-EDC dust
49.789	144.66523	2.86808	1538 MS-EDC dust
50.937	148.95161	3.44451	1538 MS-EDC dust
51.715	151.24903	3.67090	1538 MS-EDC dust
52.5	155	3.83772	1538 MS-EDC dust
55.6	181	2.58073	1538 MS-EDC dust

Supplementary Table 2. The results of grain size measurements at Sites U1537 and U1538

Number			Holocene	σ	$2\sigma/\sqrt{n}$	LGM	σ	$2\sigma/\sqrt{n}$	LIG	σ	$2\sigma/\sqrt{n}$	PGM	σ	$2\sigma/\sqrt{n}$
1	U1537(1)	Average $\overline{SS}$ (μm)	16.1	0.5	0.2	16.2	0.3	0.3	21.5	1.8	0.8	16.3	1.2	0.7
2	U1537(2)	Average $\overline{SS}$ (μm)	17.6	0.3	0.3	16.3	0.2	0.3	21.7	1.5	1.2	16.0	0.4	0.2
3	U1538	Average $\overline{SS}$ (μm)	19.0	0.8	0.5	16.6	0.3	0.4	21.5	1.6	1.1	17.8	1.2	0.8

Note that the analytical precision was ± 0.08 μm in our measurements. It is not additionally propagated into the standard error of the mean, $2\sigma/\sqrt{n}$. The numbers of first column mark the group of the grain size measurement. U1537(1) = Group One of U1537; U1537(2) = Group Two of U1537.

References

1. Weber, M.E., Raymo, M.E., Peck, V.L., Williams, T., & IODP Expedition 382 Scientists, E. Iceberg Alley and Subantarctic Ice and Ocean Dynamics. *Proceedings of the International Ocean Discovery Program*, pp. 1-32. (2021).
2. Lambert, F., Bigler, M., Steffensen, J. P., Hutterli, M., & Fischer, H. Centennial mineral dust variability in high-resolution ice core data from Dome C, Antarctica. *Clim. Past* **8**, 609-623 (2012).
3. Lu, L., Zheng, X., Chen, Z., Yan, W., Wu, S., Zheng, L., ... & Kao, S. One-to-one coupling between Southern Ocean productivity and Antarctica climate. *Geophys. Res. Lett.* **49**, e2022GL098761 (2022).
4. Lougheed, B. C., & Obrochta, S. P. A rapid, deterministic age-depth modeling routine for geological sequences with inherent depth uncertainty. *Paleoceanogr. Paleocl.* **34**, 122–133 (2019).
5. McCave, I. N., Thornalley, D. J. R., & Hall, I. R. Relation of sortable silt grain-size to deep-sea current speeds: Calibration of the 'Mud Current Meter'. *Deep Sea Res. Part I: Oceanographic Res. Pap.* **127**, 1-12 (2017)
6. McCave, I. N., & Andrews, J. T. Distinguishing current effects in sediments delivered to the ocean by ice. I. Principles, methods and examples. *Quat. Sci. Rev.* **212**, 92-107 (2019).
7. Garcia, H. E. et al. Dissolved oxygen, apparent oxygen utilization, and oxygen saturation. *World Ocean Atlas 2013* **3**, 27 (2013).
8. Zweng, M. M. et al. Salinity. *World Ocean Atlas 2013* **2**, 39 (2013)
9. Schlitzer, R. Ocean Data View http://odv.awi.de (2011)
10. Orsi, A. H., Johnson, G. C., & Bullister, J. L. Circulation, mixing, and production of Antarctic Bottom Water. *Prog. Oceanogr.* **43**, 55-109 (1999).

11. Orsi, A. H., Whitworth III, T., & Nowlin Jr, W. D. On the meridional extent and fronts of the Antarctic Circumpolar Current. *Deep Sea Res. Part I: Oceanographic Res. Pap.* **42**, 641-673 (1995).

12. Toyos, M. H., Lamy, F., Lange, C. B., Lembke-Jene, L., Saavedra-Pellitero, M., Esper, O., & Arz, H. W. Antarctic circumpolar current dynamics at the Pacific entrance to the Drake Passage over the past 1.3 million years. *Paleoceanogr. Paleoclimatol.* **35**, e2019PA003773 (2020).

13. Wu, S., Lembke-Jene, L., Lamy, F., Arz, H. W., Nowaczyk, N., Xiao, W., ... & Kuhn, G. Orbital-and millennial-scale Antarctic Circumpolar Current variability in Drake Passage over the past 140,000 years. *Nat. Commun.* **12**, 1-9 (2021).

14. McCave, I. N., Crowhurst, S. J., Kuhn, G., Hillenbrand, C. D., & Meredith, M. P. Minimal change in Antarctic Circumpolar Current flow speed between the last glacial and Holocene. *Nat. Geosci.* **7**, 113-116 (2014).

15. Bazin, L., Landais, A., Lemieux-Dudon, B., Toyé Mahamadou Kele, H., Veres, D., Parrenin, F., ... & Wolff, E. An optimized multi-proxy, multi-site Antarctic ice and gas orbital chronology (AICC2012): 120–800 ka. *Clim. Past* **9**, 1715-1731 (2013).

16. North Greenland Ice Core Project members. High resolution record of Northern Hemisphere climate extending into the last interglacial period. *Nature* **431**, 147-151 (2004).

17. Parrenin, F., Masson-Delmotte, V., Köhler, P., Raynaud, D., Paillard, D., Schwander, J., ... & Jouzel, J. Synchronous change of atmospheric CO_2 and Antarctic temperature during the last deglacial warming. *Science* **339**, 1060-1063 (2013).

18. Gottschalk, J., Skinner, L. C., Jaccard, S. L., Menviel, L., Nehrbass-Ahles, C., & Waelbroeck, C. Southern Ocean link between changes in atmospheric CO_2 levels and northern-hemisphere climate anomalies during the last two glacial periods. *Quat. Sci. Rev.* **230**, 106067 (2020).

19. Gottschalk, J., Skinner, L. C., Misra, S., Waelbroeck, C., Menviel, L., & Timmermann, A. Abrupt changes in the southern extent of North Atlantic Deep Water during Dansgaard–Oeschger events. *Nat. Geosci.* **8**, 950-954 (2015).

20. Huang, H., Gutjahr, M., Eisenhauer, A., & Kuhn, G. No detectable Weddell Sea Antarctic bottom water export during the last and penultimate glacial maximum. *Nat. Commun.* **11**, 1-10 (2020).

21. Mulet, S., Rio, M.-H., Etienne, H., Artana, C., Cancet, M., Dibarboure, G., Feng, H., Husson, R., Picot, N., Provost, C., & Strub, P. T.: The new CNES-CLS18 global mean dynamic topography, *Ocean Sci.* **17**, 789-808 (2021).

22. Ho, S. L., Mollenhauer, G., Lamy, F., Martínez-Garcia, A., Mohtadi, M., Gersonde, R., ... & Tiedemann, R. Sea surface temperature variability in the Pacific sector of the Southern Ocean over the past 700 kyr. *Paleoceanography* **27**, PA4202 (2012).

23. Peeters, F. J., Acheson, R., Brummer, G. J. A., De Ruijter, W. P., Schneider, R. R., Ganssen, G. M., ... & Kroon, D. Vigorous exchange between the Indian and Atlantic oceans at the end of the past five glacial periods. *Nature* **430**, 661-665 (2004).

24. Torrence, C., & Compo, G. P. A practical guide to wavelet analysis. *B. Am. Meteorol. Soc.* **79**, 61-78 (1998).

25. Berger, A., & Loutre, M. F. Insolation values for the climate of the last 10 million years. *Quat. Sci. Rev.* **10**, 297-317 (1991).

26. Köhler, P., Nehrbass-Ahles, C., Schmitt, J., Stocker, T. F., Fischer, H. A 156 kyr smoothed history of the atmospheric greenhouse gases CO_2, CH_4, and N_2O and their radiative forcing. *Earth Syst. Sci. Data* **9**, 363-387 (2017).

27. Ai, X. E. et al. Southern Ocean upwelling, Earth's obliquity, and glacial-interglacial atmospheric CO_2 change. *Science* **370**, 1348-1352 (2020).